Supplement of Atmos. Chem. Phys., 26, 2785–2796, 2026
https://doi.org/10.5194/acp-26-2785-2026-supplement

Atmospheric Chemistry and Physics
Open Access
EGU

Supplement of

Understanding divergent brown carbon photobleaching rates from molecular perspective

Yanting Qiu et al.

Correspondence to: Zhijun Wu (zhijunwu@pku.edu.cn)

S1. The measurement of steady-state OH radical concentration

The steady-state OH radical concentration ($[OH]_{ss}$) was measured using the peudo-first order decay of benzoic acid (BA, 98%, Alaadin Inc.). According to previous study (Hems and Abbatt, 2018), BA had a secondary order rate constant with OH radicals. The peudo-first order decay of BA, the relationship between the peudo-first order rate constant and secondary order rate constant respectively followed eq.(S1) and eq.(S2).

$$BA_t = BA_0 \times \exp(-k_{BA}^{I} t) \qquad \text{(S1)}$$

$$k_{BA}^{I} = k_{BA}^{II} \times [OH]_{ss} \qquad \text{(S2)}$$

In eqs.(S1), the BA_t and BA_0 was the concentration of BA after *t* hours of equivalent solar radiation and before photochemical aging, respectively. We conducted a series of parallel experiments to measure the $[OH]_{ss}$, i.e., samples from this set of experiments were only used to analyze the variations in the concentration of BA and not for other analysis. The secondary order rate constant for BA (k_{BA}^{II}) was 2.1×10^{13} M^{-1} h^{-1}. In this work, the measured $[OH]_{ss}$ was $(3.17 \pm 0.47) \times 10^{-14}$ M.

S2. Scaling the experimental aging time to the solar radiation in the atmosphere

To estimate the experimental photochemical aging time of BrC under the atmospheric conditions, the photodegradation rate *J* was assumed to be the convolution of spectral flux $F(\lambda)$, quantum yield $\varphi(\lambda)$, and absorption cross section $\sigma(\lambda)$ using eq. (S3):

$$J = \int F(\lambda) \times \varphi(\lambda) \times \sigma(\lambda)\, d\lambda \qquad \text{(S3)}$$

At longer wavelength, the absorption cross section and quantum yield of molecules become small (Malecha et al., 2018). Therefore, limiting the integration to the UV bulb range is reasonable, as photoreactions at longer wavelengths are minimal. For a narrow integration range, the scaling factor can be approximated as the ratio between the integrated spectral flux densities of two different light sources, as shown in eq. (S4):

$$\text{scaling factor} = \frac{\int F(\lambda)_{UV\ bulbs} d\lambda}{\int F(\lambda)_{atmosphere} d\lambda} \qquad \text{(S4)}$$

Using eq. (S4), the spectral flux densities of the UV bulbs used in this work and the 24-hour average Beijing solar spectrum at 300 m above sea level (typical altitude in Beijing) were integrated from 360 nm to 380 nm. The 24-hour average Beijing solar spectrum was simulated using the Tropospheric Ultraviolet and Visible Radiation model (TUV, https://www2.acom.ucar.edu/modeling/tropospheric-ultraviolet-and-visible-tuv-radiation-model). The setup of the TUV model is listed in Table S4, and the simulated results are displayed in Figure S3. Our calculated results showed that the scaling factor between the experimental exposure and the atmospheric solar exposure was 3.86. In this work, the scaling factor was set to 4.0 to simplify the calculation.

S3. (Semi-) Quantification of BrC chromophores using non-target analysis

In this work, we analyzed the molecular composition of p-BrC based on non-target analysis (NTA) approach. Table S2 summarizes the sampling details of ambient $PM_{2.5}$ samples. We analyzed the molecular composition of p-BrC samples following the identical approach described in our previous work (Qiu et al., 2024). Briefly, the NTA approach was adopted using the UHPLC system (Thermo Ultimate 3000, Thermo Scientific) coupled with

HRMS. The sample extraction was analyzed with full scan and higher-energy collisional dissociation (HCD) modes to obtain their MS and MS^2 spectra. Chromatographic separation was performed on a reversed-phase column (Accucore C18, 100×2.1 mm, 2.6 μm particle size, Thermo Scientific) with a flow rate of 0.3 mL/min and an injection volume of 2 μL. Both mobile phase A (water) and B (methanol) contained 2 mM ammonium acetate. The HPLC gradient program was as follows: starting at 5% B, increasing linearly to 25% B from 1.0 to 7.0 minutes, then to 95% B by 20.0 minutes, holding for 2 minutes, and returning to 5% B with a 6-minute hold before the next injection. The Orbitrap HRMS was operated in ESI(-) mode. The settings were as follows: capillary voltage -3.0 kV, capillary temperature 320°C, vaporizer temperature 35°C, and sheath, auxiliary, and sweep gas at 2, 1, and 1 arbitrary units, respectively.

The detected species were classified into five organic compound groups (acyl compounds (ACs), carboxylic acids (CAs), organonitrates (ONs), nitrophenols (including phenols, NPs), and organosulfates (OSs)) based on elemental composition and MS^2 spectra. The mass concentration of different groups of organic compounds listed in Table 1 of the main text was quantified using the external standard method. Mixture solutions containing imidazole-2-carboxaldehyde (2-IC), benzaldehyde, 3-nitrosalicylic acid (3-NA), sorbic acid (SA), 4-nitrophenol (4-NP), 4-nitrocatechol (4-NC), and 3-amino-4-methoxy-toluene-6-sulfonic acid (3,4,6-AMTSA) were prepared at concentrations of 1 ng/mL, 5 ng/mL, 10 ng/mL, 20 ng/mL, 50 ng/mL, 0.1 μg/mL, 0.5 μg/mL, and 1 μg/mL. All of these standards exhibit strong correlation with their fitted calibration curves ($R^2 > 0.999$).

Figure S4 shows the molecular composition and relevant solar radiation during sampling, which is represented by the 75^{th} percentile solar radiation (Rad_{75}). As displayed in Table S2 and Figure S4, the sampling occurred predominantly during nighttime or under low Rad_{75}, resulting in minimal photobleaching of p-BrC prior to analysis. In addition, the molecular composition, particularly the presence of nitrophenols, is indicative of primary emissions from sources such as biomass burning and vehicle emissions, rather than secondary formation.

Table S1 The concentrations of OC, EC, and TOC of each biomass burning $PM_{2.5}$ sample

Sample	OC ($\mu g/m^3$)	EC ($\mu g/m^3$)	TOC ($\mu g/m^3$)
Corn Straw-1	1900.29	1835.05	830.60
Corn Straw-2	1997.20	1539.04	704.54
Corn Straw-3	1348.73	1006.39	753.89
Corn Straw-4	1890.32	1582.93	854.89

Table S2 Sampling details of ambient $PM_{2.5}$ samples used for p-BrC extraction in this work

Sampling ID	Samping time*	Average $PM_{2.5}$ ($\mu g/m^3$)
20201224	10:00–9:00 +1	21.6
20201225	10:00–9:00 +1	27.0
20201226	10:00–9:00 +1	55.6
20201227	10:00–9:00 +1	73.5
20201228	10:00–9:00 +1	42.5

*: +1 indicates the next day

Table S3 The average mass concentration of $PM_{2.5}$, concentration of gaseous pollutants, ambient RH, and chemical composition in NR-PM_1 during the sampling period of $PM_{2.5}$ filters for the isolation of BrC

species (unit)	average (± standard deviation)
$PM_{2.5}$ (μg/m^3)	53.46 (± 20.97)
O_3 (ppb)	10.94 (± 9.27)
SO_2 (ppb)	1.36 (± 1.17)
CO (ppm)	0.72 (± 0.31)
NO_2 (ppb)	24.77 (± 12.34)
RH (%)	43.21 (± 19.58)
sulfate (μg/m^3)	3.79 (± 2.57)
nitrate (μg/m^3)	11.33 (± 7.65)
organics (μg/m^3)	12.64 (± 6.64)

Table S4 Setup of the TUV model

Parameter	Model setup
Latitude	39.92
Longitude	116.33
Date and time	June 20th, 2022
Overhead ozone	300 du
Surface albedo	0.1
Ground altitude	0 km
Measured altitude	0.3 km
Clouds optical depth/base/top	0.00/4.00/5.00
Aerosols optical depth/S-S albedo/alpha	0.235/0.990/1.000
Sunlight direct beam/diffuse down/diffuse up	1.0/1.0/1.0

Table S5 The MAC, calculated k_{BrC}, and corresponding references of Figure 1(b) in the main text

BrC Type	MAC ($cm^2\ g^{-1}$)	k_{BrC} (h^{-1})	Reference
aq-BrC	7548.68	1.13	this work
p-BrC	787.66	0.10	
b-BrC	9340.82	0.05	
aq-BrC	6300	4.02	(Müller et al., 2023)
SRFA	32000	0.007	
b-BrC	10000	0.07	
p-BrC	400	0.08	
b-BrC	6400	0.05	(Hems et al., 2020)
4-nitrocatechol	12000	0.04	(Hems and Abbatt, 2018)
aq-BrC	4200	6.60	(Aiona et al., 2017)
Limonene-O_3-SOA	800	2.28	
CDOM	26000	0.02	(Borduas-Dedekind et al., 2019)
b-BrC	7000	0.07	(Fleming et al., 2020)
b-BrC	6300	0.04	(Wong et al., 2019)
p-BrC	650	0.08	(Qiu et al., 2024)
2,4-dinitrophenol	11000	0.05	(Liu et al., 2025)
3-nitrocatechol	10000	0.04	
Wood smoke SOA	8000	0.18	(Liu-Kang et al., 2022)
b-BrC	7600	0.20	(Choudhary et al., 2023)
b-BrC	14000	0.02	(Fan et al., 2020)
aq-BrC	2200	0.85	(Gao and Zhang, 2019)

Table S6 Detected products after photochemical aging for aq-BrC

m/z	elemental composition	chemical structure	MS^2 fragments
99.01	$C_4H_4O_3$	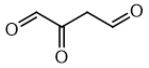	-*
113.02	$C_5H_6O_3$	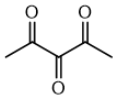	95, 61
125.04	$C_5H_6O_2N_2$	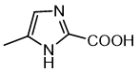	81, 72
139.05	$C_6H_8O_2N_2$	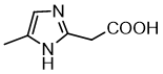	95, 69, 59
167.05	$C_7H_8O_3N_2$	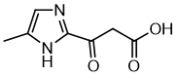	123, 59
180.05	$C_8H_9O_3N_2$	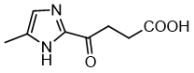	137, 109, 81
189.08	$C_8H_{14}O_5$	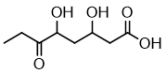	115, 71, 59
195.08	$C_9H_{12}O_3N_2$	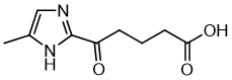	151, 123, 97, 81
213.08	$C_{10}H_{14}O_5$	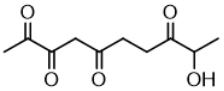	195, 127, 85

*: The MS^2 fragments were not available due to low signal intensities of parent ions or the *m/z* of MS^2 fragments were below the lower limit of instrument

Table S7 Detected products after photochemical aging for p-BrC

m/z	elemental composition	chemical structure	MS^2 fragments
111.01	$C_5H_4O_3$	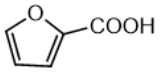	67
115.00	$C_4H_4O_4$	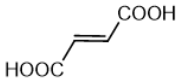	71, 68
141.03	$C_5H_6O_3N_2$	-	-
165.02	$C_8H_6O_4$	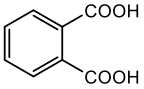	93
166.05	$C_8H_9NO_3$	-	-
168.98	$C_3H_6O_6S$	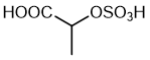	125, 97
182.01	$C_7H_5NO_5$	-	-
186.00	$C_6H_5O_6N$	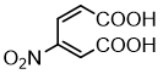	141, 124, 95
190.04	$C_6H_9O_6N$	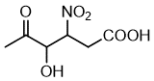	145, 99
202.00	$C_6H_5O_7N$	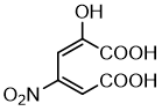	158, 141, 130
208.06	$C_{10}H_{11}NO_4$	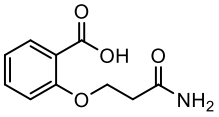	137, 93
217.99	$C_6H_5O_8N$	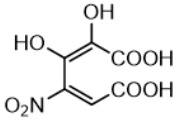	173, 127, 100, 72
233.99	$C_6H_5O_9N$	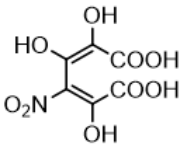	189, 144, 116, 73
240.05	$C_{10}H_{11}O_6N$	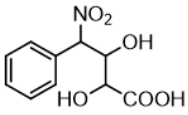	195, 162, 149

Table S7 Continued

m/z	elemental composition	chemical structure	MS^2 fragments
246.02	$C_8H_9O_8N$	-	201, 130, 114, 69
248.03	$C_7H_{11}O_5N_3S$	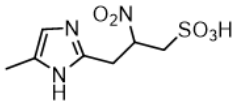	153, 136, 81

84 **Table S8** Detected products after photochemical aging for b-BrC

m/z	elemental composition	chemical structure	MS^2 fragments
111.01	$C_5H_4O_3$	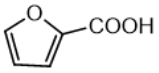	67
149.02	$C_8H_6O_3$	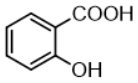	93, 65
165.02	$C_8H_6O_4$	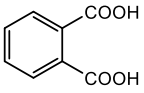	93
166.05	$C_8H_9O_3N$	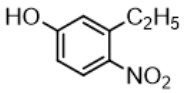	-
183.04	$C_{12}H_8O_2$	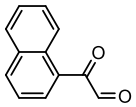	127, 101, 77
186.00	$C_6H_5O_6N$	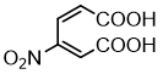	141, 124, 95
190.04	$C_6H_9O_6N$	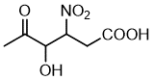	145, 99
202.00	$C_6H_5O_7N$	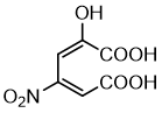	158, 141, 130
208.06	$C_{10}H_{11}NO_4$	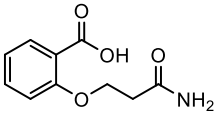	137, 93
217.99	$C_6H_5O_8N$	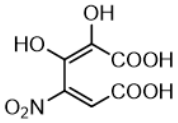	173, 127, 100, 72
225.09	$C_{15}H_{14}O_2$	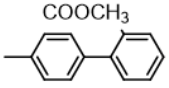	193, 167, 141
233.99	$C_6H_5O_9N$	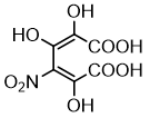	189, 144, 116, 73

85

Table S8 Continued

m/z	elemental composition	chemical structure	MS^2 fragments
244.03	$C_8H_9O_7N_2$	-	-
335.05	$C_{14}H_{12}N_2O_8$	-	-
391.08	$C_{15}H_{16}O_5N_6S$	-	-

Figure S1 Typical sample collection process of biomass burning $PM_{2.5}$ samples

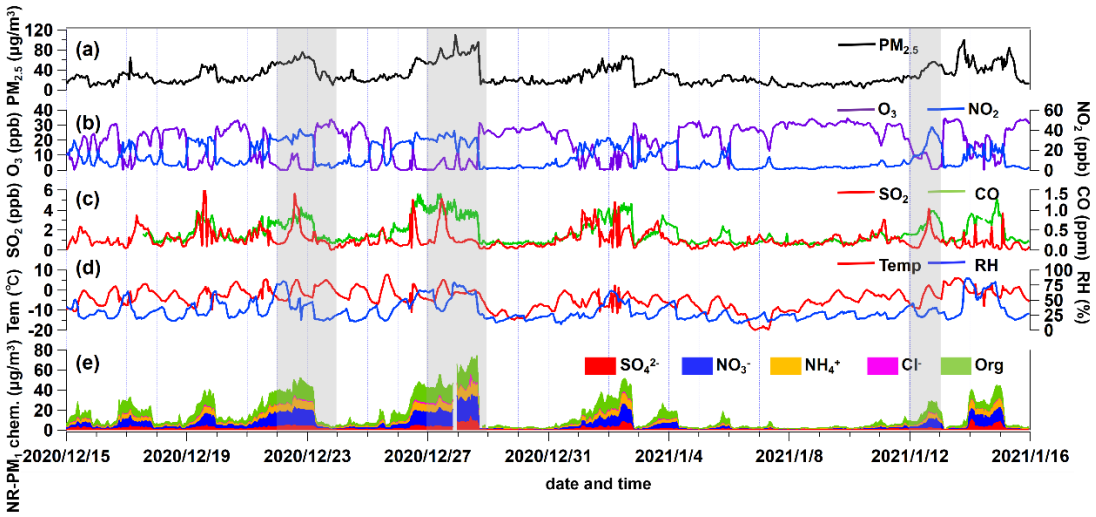

Figure S2 Time series of gaseous pollutants concentrations, $PM_{2.5}$ mass concentrations, chemical composition of NR-PM_1, and meteorological parameters during the field observation.

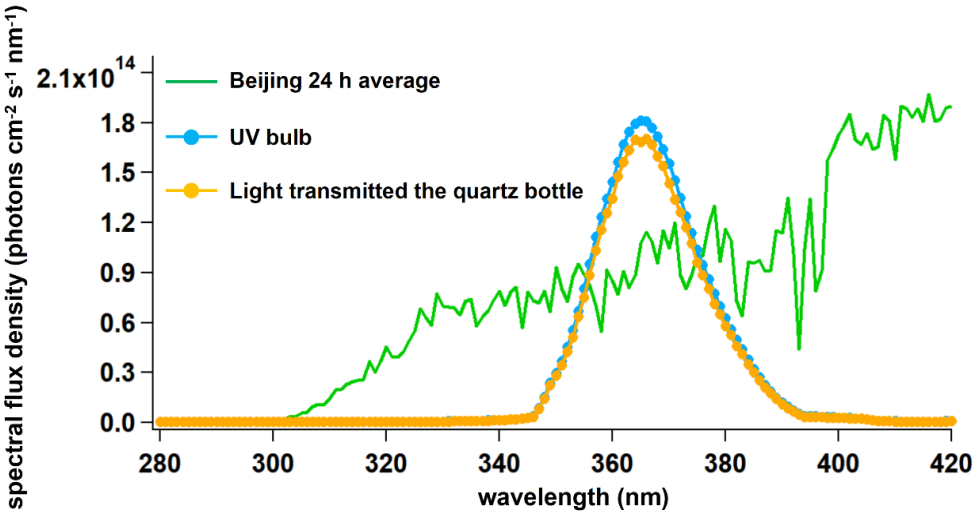

Figure S3 The comparison between the radiation used in laboratory photochemical aging experiment and solar radiation

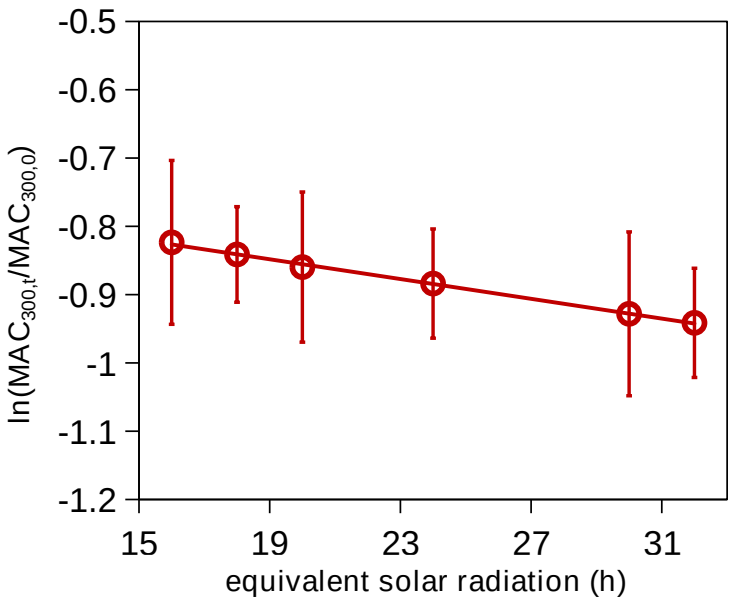

Figure S4 The variations in ln($MAC_{300,t}/MAC_{300,0}$) of b-BrC when the equivalent solar radiation was expanded to 32 h

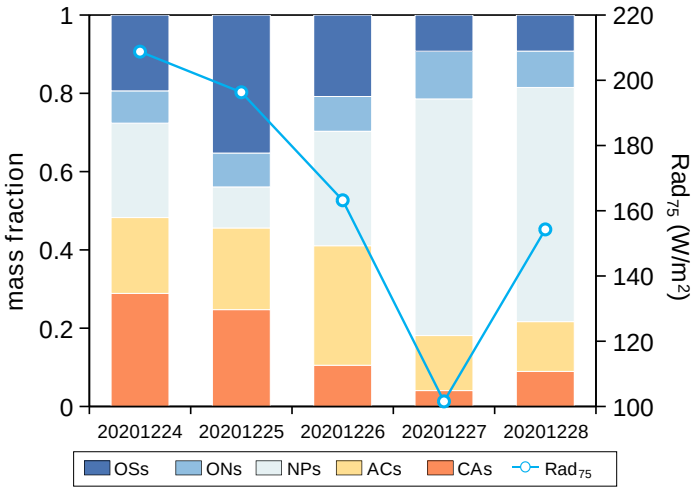

Figure S5 The mass fractions of 5 groups of identified species and Rad_{75} for p-BrC

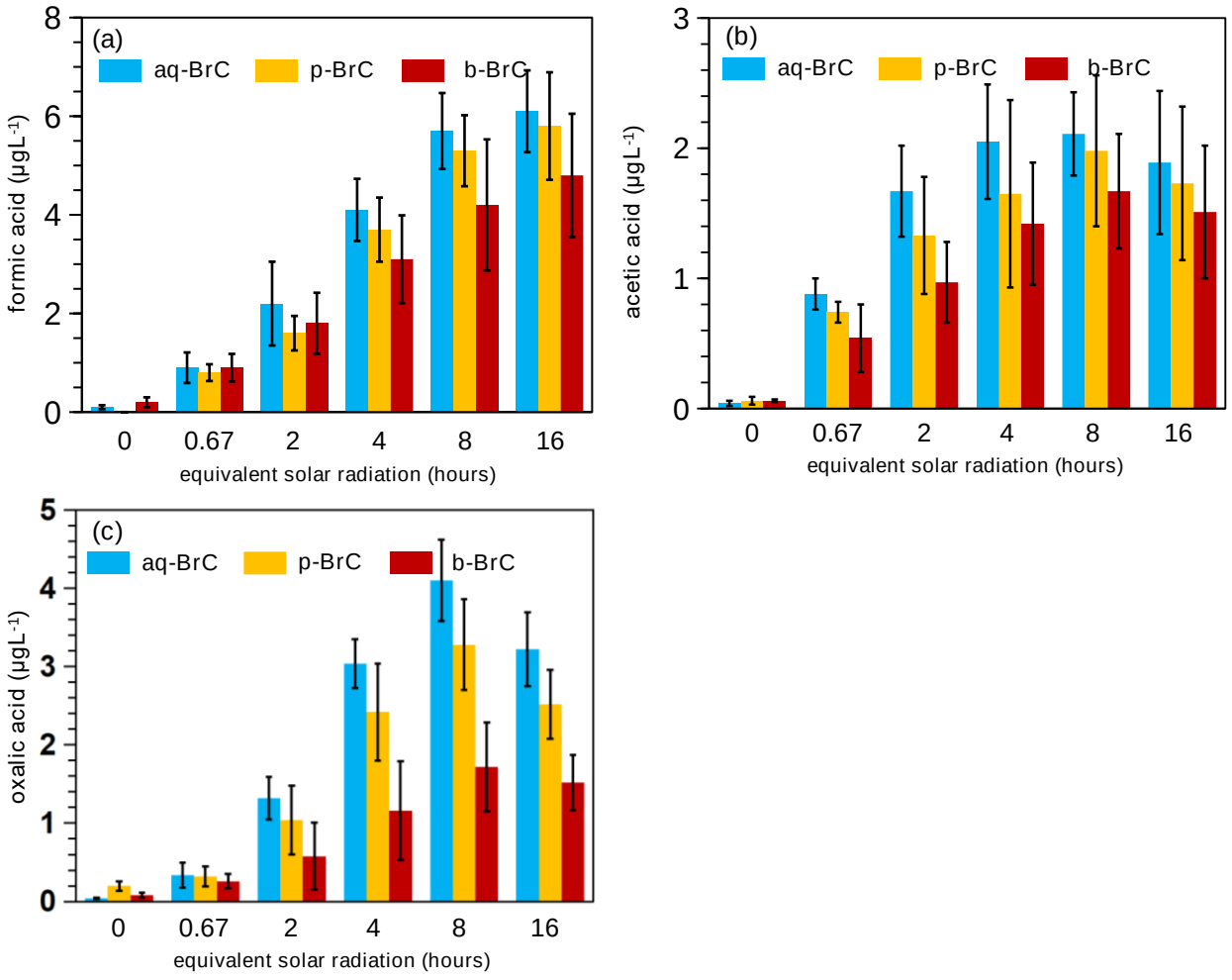

106

107 **Figure S6** The variations in (a) formic acid, (b) acetic acid, and (c) oxalic acid as a function of
108 equivalent solar radiation hours. The legend was shared in all panels.

109

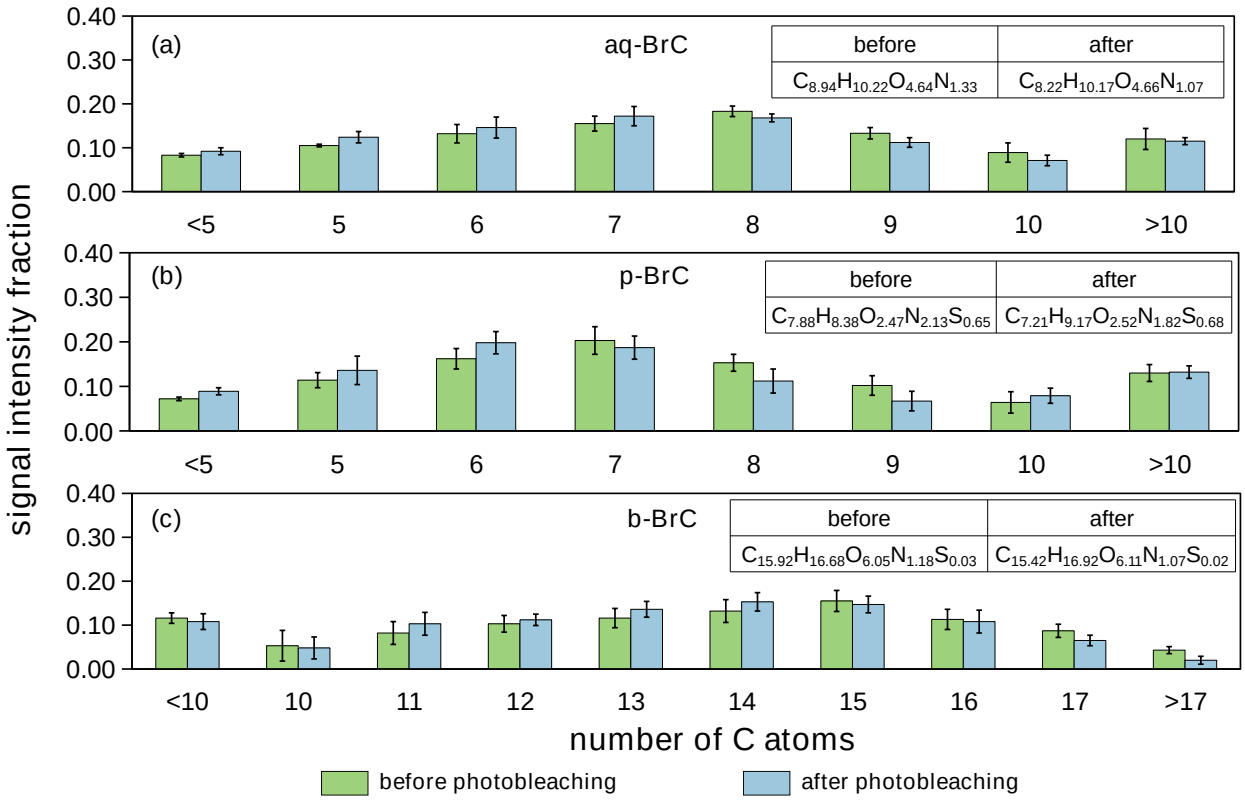

Figure S7 The signal intensity fraction distributions of detected compounds with different number of C atoms before and after photobleaching for (a) aq-BrC, (b) p-BrC, and (c) b-BrC. Error bars represent one standard deviation of datapoints derive from three (aq-BrC and b-BrC) or five (p-BrC) parallel experiments. The inserted tables are signal-intensity-weighted average elemental composition of BrC.

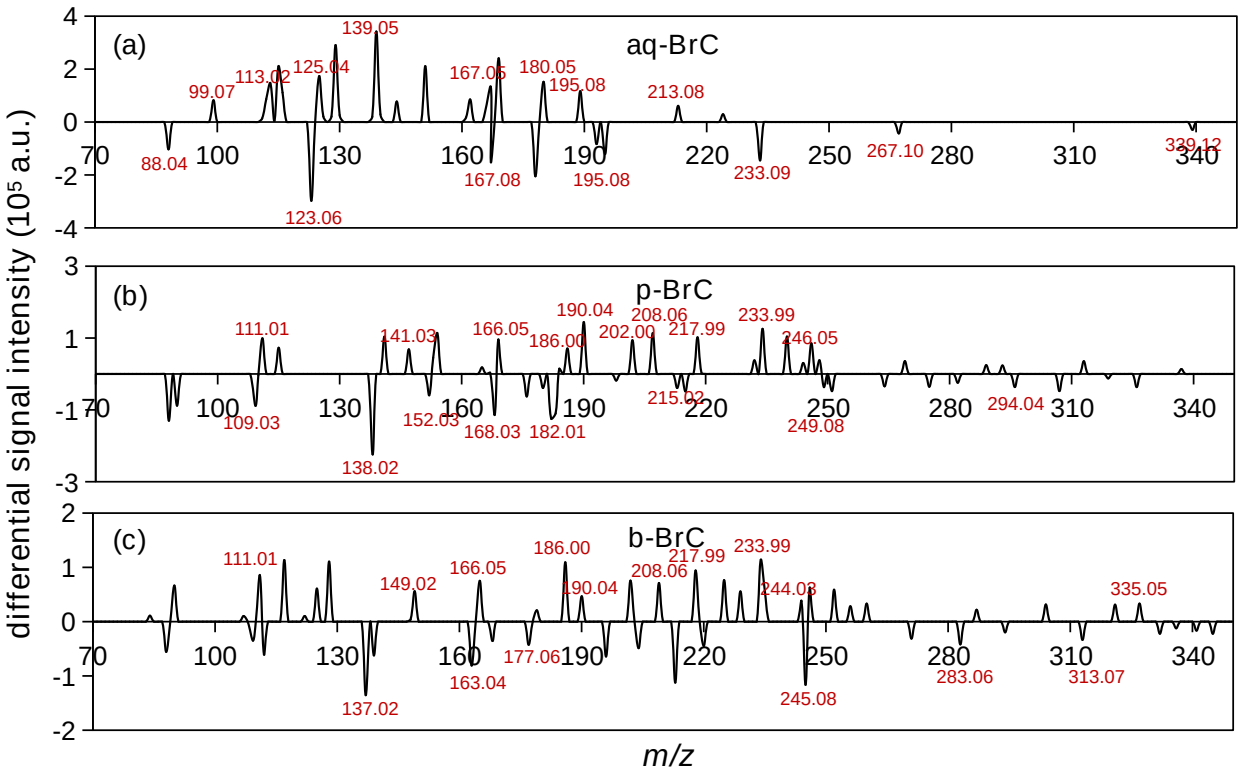

Figure S8 The differential HRMS spectra of (a) aq-BrC, (b) p-BrC, and (c) b-BrC before and after photobleaching. The positive and negative peaks respectively represent signal intensities increase and decrease after photobleaching.

SI References

Aiona, P. K., Lee, H. J., Leslie, R., Lin, P., Laskin, A., Laskin, J., and Nizkorodov, S. A.: Photochemistry of Products of the Aqueous Reaction of Methylglyoxal with Ammonium Sulfate, ACS Earth and Space Chemistry, 1, 522-532, https://doi.org/10.1021/acsearthspacechem.7b00075, 2017.

Borduas-Dedekind, N., Ossola, R., David, R. O., Boynton, L. S., Weichlinger, V., Kanji, Z. A., and McNeill, K.: Photomineralization mechanism changes the ability of dissolved organic matter to activate cloud droplets and to nucleate ice crystals, Atmospheric Chemistry and Physics, 19, 12397-12412, https://doi.org/10.5194/acp-19-12397-2019, 2019.

Choudhary, V., Roson, M. L., Guo, X., Gautam, T., Gupta, T., and Zhao, R.: Aqueous-phase photochemical oxidation of water-soluble brown carbon aerosols arising from solid biomass fuel burning, Environmental Science: Atmospheres, 3, 816-829, https://doi.org/10.1039/D2EA00151A, 2023.

Fan, X., Cao, T., Yu, X., Wang, Y., Xiao, X., Li, F., Xie, Y., Ji, W., Song, J., and Peng, P.: The evolutionary behavior of chromophoric brown carbon during ozone aging of fine particles from biomass burning, Atmospheric Chemistry and Physics, 20, 4593-4605, 10.5194/acp-20-4593-2020, 2020.

Fleming, L. T., Lin, P., Roberts, J. M., Selimovic, V., Yokelson, R., Laskin, J., Laskin, A., and Nizkorodov, S. A.: Molecular composition and photochemical lifetimes of brown carbon chromophores in biomass burning organic aerosol, Atmospheric Chemistry and Physics, 20, 1105-1129, https://doi.org/10.5194/acp-20-1105-2020, 2020.

Gao, Y., and Zhang, Y.: Optical properties investigation of the reactions between methylglyoxal and glycine/ammonium sulfate, Spectrochimica Acta Part A: Molecular and Biomolecular Spectroscopy, 215, 112-121, https://doi.org/10.1016/j.saa.2019.02.087, 2019.

Hems, R. F., and Abbatt, J. P. D.: Aqueous Phase Photo-oxidation of Brown Carbon Nitrophenols: Reaction Kinetics, Mechanism, and Evolution of Light Absorption, ACS Earth and Space Chemistry, 2, 225-234, https://doi.org/10.1021/acsearthspacechem.7b00123, 2018.

Hems, R. F., Schnitzler, E. G., Bastawrous, M., Soong, R., Simpson, A. J., and Abbatt, J. P. D.: Aqueous Photoreactions of Wood Smoke Brown Carbon, ACS Earth and Space Chemistry, 4, 1149-1160, https://doi.org/10.1021/acsearthspacechem.0c00117, 2020.

Liu-Kang, C., Gallimore, P. J., Liu, T., and Abbatt, J. P. D.: Photoreaction of biomass burning brown carbon aerosol particles, Environmental Science: Atmospheres, 2, 270-278, https://doi.org/10.1039/d1ea00088h, 2022.

Liu, Y., Huang, R.-J., Lin, C., Yuan, W., Li, Y. J., Zhong, H., Yang, L., Wang, T., Huang, W., Xu, W., Huang, D. D., and Huang, C.: Nitrate-Photolysis Shortens the Lifetimes of Brown Carbon Tracers from Biomass Burning, Environmental Science & Technology, 59, 640-649, https://doi.org/10.1021/acs.est.4c06123, 2025.

Malecha, K. T., Cai, Z., and Nizkorodov, S. A.: Photodegradation of Secondary Organic Aerosol Material Quantified with a Quartz Crystal Microbalance, Environmental Science & Technology Letters, 5, 366-371, 10.1021/acs.estlett.8b00231, 2018.

Müller, S., Giorio, C., and Borduas-Dedekind, N.: Tracking the Photomineralization Mechanism in Irradiated Lab-Generated and Field-Collected Brown Carbon Samples and Its Effect on Cloud Condensation Nuclei Abilities, ACS Environmental Au, 3, 164-178, https://doi.org/10.1021/acsenvironau.2c00055, 2023.

Qiu, Y., Qiu, T., Wu, Z., Liu, Y., Fang, W., Man, R., Liu, Y., Wang, J., Meng, X., Chen, J., Liang, D., Guo, S., and Hu, M.: Observational Evidence of Brown Carbon Photobleaching in Urban Atmosphere at Molecular Level, Environmental Science and Technology Letters, 11, 1032-1039, https://doi.org/10.1021/acs.estlett.4c00647, 2024.

Wong, J. P. S., Tsagkaraki, M., Tsiodra, I., Mihalopoulos, N., Violaki, K., Kanakidou, M., Sciare, J., Nenes, A., and Weber, R. J.: Atmospheric evolution of molecular-weight-separated brown carbon from biomass burning, Atmospheric Chemistry and Physics, 19, 7319-7334, https://doi.org/10.5194/acp-19-7319-2019, 2019.